JTTEE5 6:217-227

Alumina Grit Blasting Parameters for Surface Preparation in the Plasma Spraying Operation

M. Mellali, A. Grimaud, A.C. Leger, P. Fauchais, and J. Lu

This paper examines how the grit blasting process influences the surface roughness of different substrates, the grit residue, and the grit erosion. The influence of grit blasting conditions on induced substrate residual stresses is also discussed. Aluminum alloy, cast iron, and hard steel were blasted with white alumina grits of 0.5, 1, and 1.4 mm mean diameters. Grit blasting was performed using either a suction-type or a pressure-type machine equipped with straight nozzles made of B_4C. The influence of the following parameters was studied: grit blasting distance (56 to 200 mm), blasting time (3 to 30 s), angle between nozzle and blasted surface (30°, 60°, 90°), and blasting pressure (0.2 to 0.7 MPa). The roughness of the substrate was characterized either by using a perthometer or by image analysis. The grit residue remaining at the blasted surface was evaluated after cleaning by image analysis. The residual stresses induced by grit blasting were determined by using the incremental hole drilling method and by measuring the deflection of grit-blasted beams.

Grit size was determined to be the most important influence on roughness. The average values of R_a and R_t and the percentage of grit residue increased with grit size as well as the depth of the plastic zone under the substrate. An increase of the pressure slightly increased the values of R_a and R_t but also promoted grit breakdown and grit residue.

A blasting time of 3 to 6 s was sufficient to obtain the highest roughness and limit the grit breakdown. The residual stresses generated under the blasted surface were compressive, and the depth of the affected zone depended on the grit diameter, the blasting pressure, and the Young's modulus of the substrate. Moreover, the maximum residual stress was reached at the limit of the plastic zone (i.e., several tenths of a millimeter below the substrate surface).

Keywords grit blasting procedure roughness, residual stresses, surface preparation

1. Introduction

SURFACE preparation is the most critical step in a plasma spraying operation (Ref 1). Coating adhesion quality is directly related to the cleanliness and roughness of the substrate surface, especially when spraying onto cold substrates (Ref 1-6). Grit blasting is generally used to roughen the substrate surface to obtain better mechanical adhesion of the coating to the substrate. Other than the abrasive nature and size, blasting conditions are critical to (1) the surface roughness achieved, (2) the quantity of embedded abrasive particles (which has a potential negative effect on the adhesion of the coatings), and (3) the abrasive wear (which increases the grit blasting cost and the quantity of embedded particles) (Ref 7-14). The main grit blasting parameters are the nature, shape (particles with blocky and angular shapes afford greater cutting action), and size distribution of the abrasive. Important features of the blasting procedure are the type of machine (in most cases suction or pressure type), nozzle internal diameter, air pressure, blasting angle, blasting distance, blasting time, and abrasive recycling. Few data are available in the literature, and only several studies are directly applicable to plasma spray (e.g., Ref 7 and 15).

This paper examines which variables of the grit blasting process most influence surface roughness and grit wear so that these variables can be controlled to obtain reproducible roughnesses. The influence of these variables on substrate contamination and the effectiveness of the cleaning procedure (air blast followed by ultrasonic cleaning) is also examined. The number of variables was limited by selecting one grit. Usually, alumina or silicon carbide grits are used in plasma spraying because these materials result in sharp peaks and undercuts that appear favorable to coating adhesion. The results of Yankee et al. (Ref 15) show that the wear of SiC is more important than that of Al_2O_3. The surface roughness values obtained with SiC are significantly lower than those obtained with Al_2O_3, which are also more regular. Thus, only Al_2O_3 grit was used in the following studies.

2. Experiment Setups

2.1 *Blasting Machines*

Two types of machines were used: (1) a suction-type machine (STM) built at the laboratory and equipped with a straight boron carbide nozzle with an 8 mm internal diameter (ID), and (2) a pressure-type machine (PTM) manufactured by Rivolta, also equipped with a cylindrical 8 mm ID B_4C nozzle.

These two machines were equipped with translation and rotation movements (see Fig. 1). The velocities could be varied between 1 and 20 mm/s for translation and 0 and 150 rev/min for

M. Mellali, A. Grimaud, A.C. Leger, and **P. Fauchais,** Equipe "Plasma, Laser, Matériaux," LMCTS, URA CNRS 320, Faculté des Sciences, University of Limoges, 123, Av. Albert Thomas, 87060 Limoges Cedex, France; **J. Lu,** Laboratoire de Mécanique, University of Troyes, 13, Blv. Henri Barbune, 12000 Troyes, France.

rotation. Moveable switches allowed the translation movement to be reversed and control of the number of nozzle passages in front of the samples or the sample holder. In the following, the translation velocity was optimized to achieve the optimum roughening and then kept constant. The corresponding blasting time was then increased by varying the number of passes of the nozzle in front of one sample. The nozzle could be fixed at different heights to vary the blasting distance between 55 and 255 mm. The rotation of the nozzle varied the blasting angle from 90° to 45°.

The air was compressed with a screw compressor followed by a 2 m^3 tank. The air was cooled at 3 °C to reduce humidity, before passing through an oil filter. The air pressure could be varied between 0.2 and 0.7 MPa, and the maximum flow rate was 40 scmh.

2.2 *Substrate Samples*

To check the effect of the substrate roughness on plasma-sprayed oxide coatings, the tensile adhesion test DIN-50160 was used (Ref 6, 16). The grit-blasted samples were disk shaped, 25 mm in diameter and 4 mm in thickness. Three materials were chosen: (1) a soft aluminum alloy AU4G (0.5 wt% Mn, 4.1% Cu, 0.7% Mg), (2) a hard carbon steel 100C6 (1.3 to 1.6 wt% Cr, 0.95 to 1.1% C, 0.4% Mn) annealed for 2 h at 800 °C and quenched in oil, and (3) a cast iron FT25 of intermediate hardness (2.8 to 3.5 wt% C, 2.8 to 3.2% Mn, 0.03 to 0.05% S). The corresponding Young's moduli and Vickers hardnesses (5 N load) are summarized in Table 1. These samples were placed in an appropriate holder that allowed attachment to the grit blasting rig.

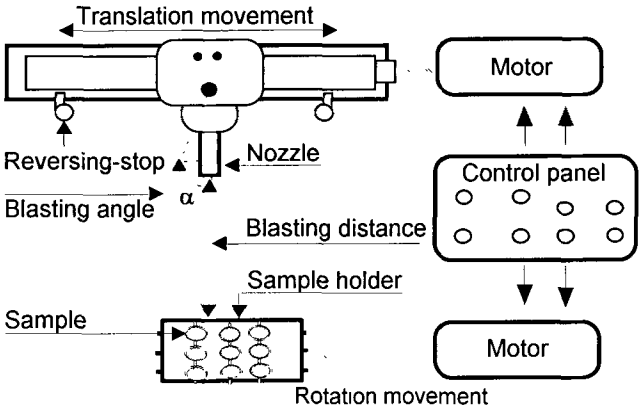

Fig. 1 Setup for sample and blasting gun displacements

2.3 *Grit Sizes*

Three sizes of white alumina (Cristalba Pechiney, France) were chosen with standard sizes of 0.5, 1, and 1.4 mm. Figure 2 shows scanning electron microscope (SEM) images of the 1.4 and 0.5 mm sizes, and Fig. 3 presents the size distributions measured with sieves. In most of the experiments, after one pass the grit was changed so that blasting was always performed with new grit. However, in some tests the same grit was reused to assess the influence of the blasting parameters on grit wear, roughness, and residues left on the blasted surface.

2.4 *Surface Roughness Characterization*

Two surface roughness parameters, both quantities expressed in micrometers, were measured:

- R_a, defined by:

$$R_a = \frac{1}{l_m}\int_0^1 |y|\,dx \qquad \text{(Eq 1)}$$

Table 1 Substrate Young's moduli and Vickers hardnesses

Material	Young's modulus, MPa	Vickers hardness (5 N load), HV
AU4G	70-74	114 ± 4
FT25	80-125	189 ± 20
100C6	210-230	946 ± 50

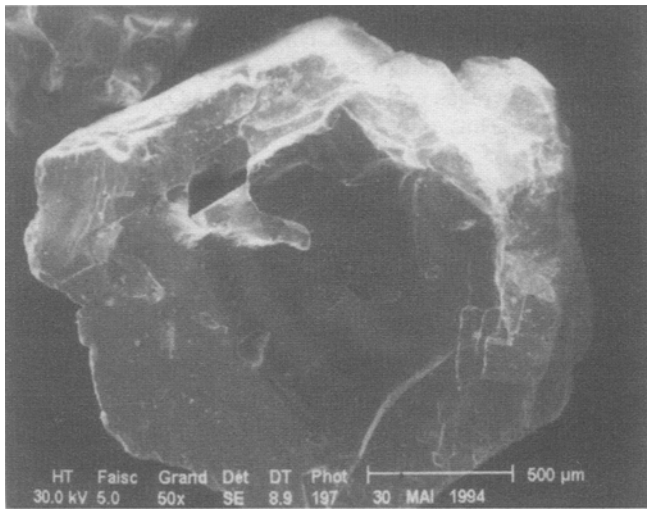

(a)

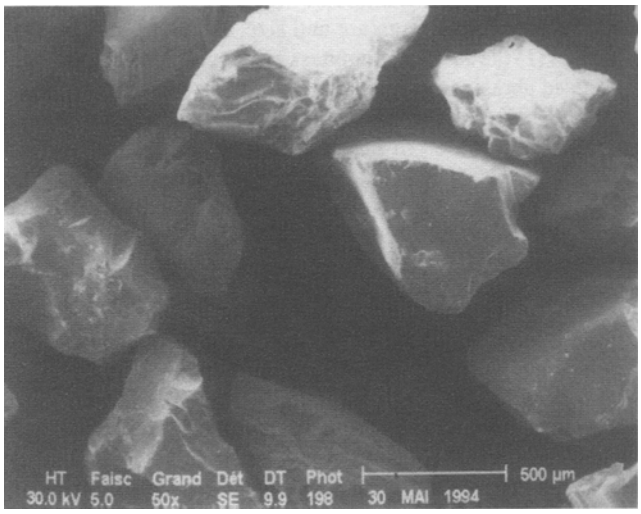

(b)

Fig. 2 SEM micrographs of alumina grits. (a) 1.4 mm grit size. (b) 0.5 mm grit size

where l_m is the analyzed length, x is the direction of the measurement, and $|y|$ is the height of the peaks and valleys along l_m (see Fig. 4).

- R_t, which is the difference in height between the highest peak and the deepest undercut (see Fig. 4).

These two quantities were measured either by using a perthometer or by image analysis. The perthometer (Mitutoyo Surftest-201; Mitutoyo, Z.I. Paris Nord, 95957 Roissy CDG Cedex, France) was equipped with a 5 μm radius diamond. It was calibrated with a calibration surface (R_a, ~3 μm; R_t, ~9.6 μm) and moved horizontally at 0.05mm/s.

For image analysis, the samples were embedded in Mecaprex SS resin (Mecaprex, Presi, 38320 Brie et Angonnes, France), then diamond cut (starting from the non-grit-blasted surface) before being polished first with SiC abrasives (sizes varying successively from 305, 500, 1000, to 1200, with 5 min polishing time for each disk at a load of 3 N). Finally, these samples were polished with diamond-impregnated cloths (with successive sizes of 6, 3, and 1 μm) for 3 min each. A specific procedure was developed to determine R_a by image analysis (Ref 16). The mean R_a and R_t values (of 20 measurements) obtained by both methods were the same within 7% (Table 2).

Each R_a value presented in the following discussion is a mean value resulting from measurements performed along 20 parallel directions. The error bars in the figures correspond to the standard deviation.

2.5 *Stress Measurement after Grit Blasting*

Grit blasting induces compressive residual stresses, which depend strongly on the blasted material, blasting conditions, and grit size (Ref 16). These stresses are distributed in a very thin layer beneath the surface (Ref 17). The resulting stress distribution within the samples can be determined by the incremental hole drilling method (Ref 17, 18) or a modified layer-removal method (Ref 19). In the present work, except for one sample where the incremental hole drilling method was used, the simple bending method of a flat beam was chosen (Ref 16). A 34CD4 steel, which has a Young's modulus (200 GPa) close to that of cast iron FT25, was used for these measurements. The beams were 2 by 10 by 100 mm^3 and were grit blasted on one side.

The curvature measurement allowed determination of the residual stress generated within the substrate, but provided no information about the stress distribution. Thus, these stress measurements can be considered indicative of the residual stress evolution with the grit blasting parameters.

Table 2 Comparison between roughnesses obtained with the perthometer and by image analysis
Results are for specimens blasted under identical conditions.

Technique	$\overline{R}_a$, μm	$\overline{R}_t$, μm
Perthometer	13.7 ± 4.2	101.6 ± 38
Image analysis	14.7 ± 4.5	94.0 ± 33

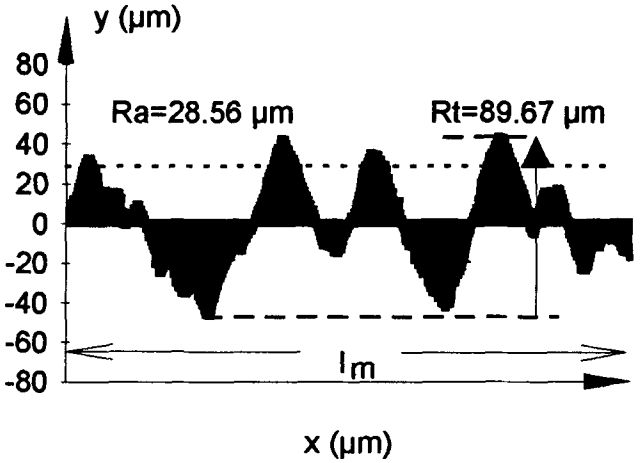

Fig. 4 Scheme of surface roughness with the definition of R_a and R_t

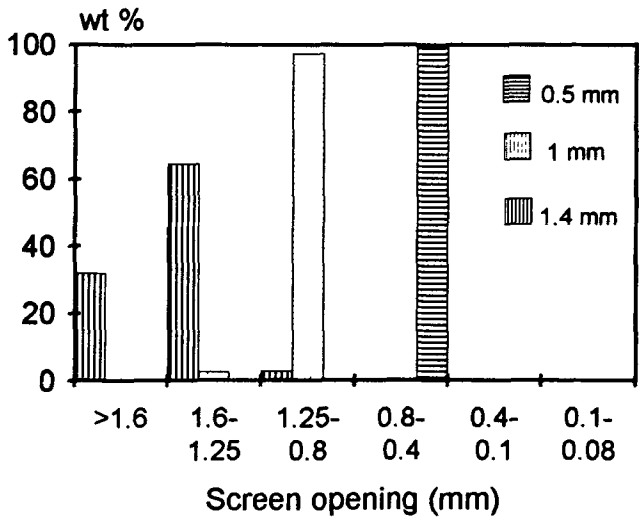

Fig. 3 Size distribution of the three alumina grits

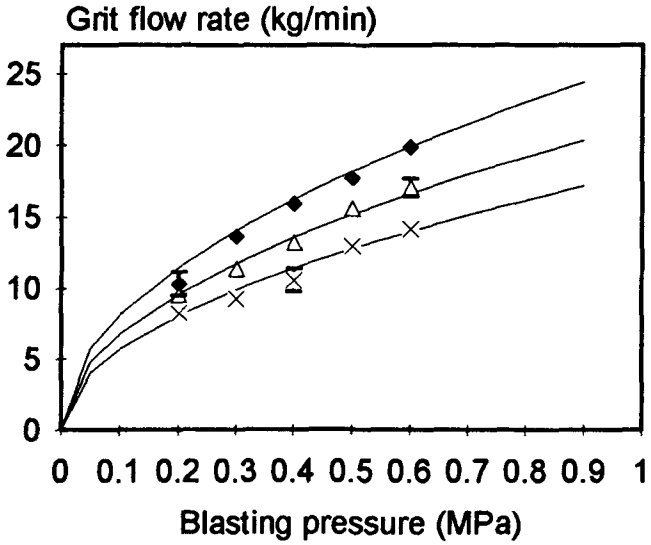

Fig. 5 Evolution with blasting pressure (p) of the grit flow rate (mg^0) for three grit sizes (PTM); ◆ = 0.5 mm, Δ = 1 mm, × = 1.4 mm

2.6 *Residue Contamination*

Contamination of the grit-blasted surface by grit residue was determined by image analysis. The white embedded alumina particles were clearly seen and their total surface S' determined as the contamination ratio CR, defined by:

$$CR = \left(\frac{S'}{S}\right) \times 100 \qquad \text{(Eq 2)}$$

where S is the substrate surface area. This measurement of residual contamination was performed after a cleaning procedure of blasting with compressed air at 0.5 MPa on the sample surface for 20 s and 4 min of ultrasonic agitation in an acetone bath solution.

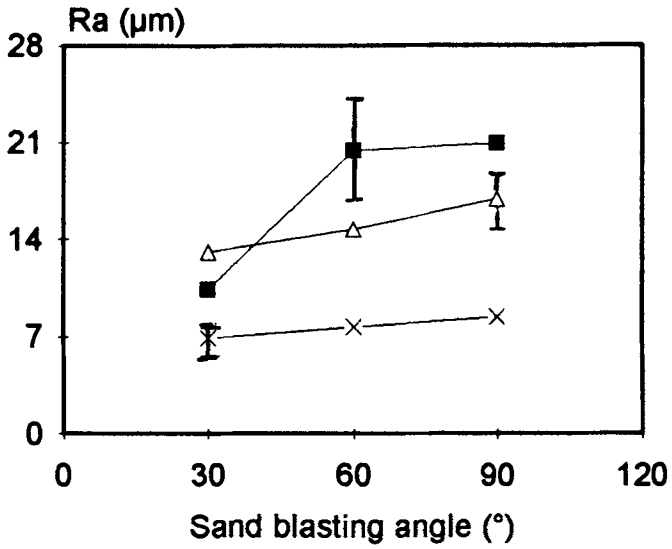

Fig. 6 Influence of grit blasting angle (Al_2O_3, D ~ 1.4 mm, p = 0.8 MPa, blasting distance d = 100 mm); ■ = AU4G, Δ = 100 C6, × = 1006T

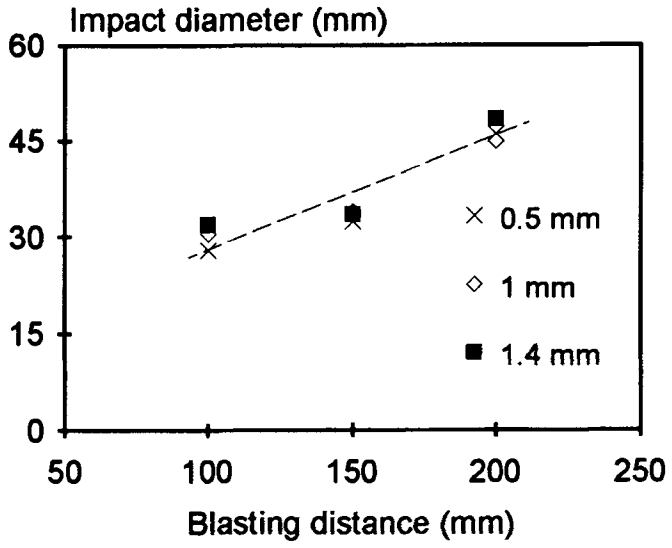

Fig. 7 Impact diameter (d_i) of the particles with respect to the grit blasting distance for p = 0.3 MPa and three grit sizes (PTM)

3. General Considerations

3.1 *Comparison of the Blasting Machines*

In both cases, as illustrated for a PTM in Fig. 5, which represents the grit flow rate, mg^0, versus the blasting pressure (in the range of 0.2 to 0.6 MPa) for the three grit sizes, mg^0 varies almost as the square root of blasting pressure, p. This leads to the following empirical relationship (valid between 0.2 and 0.6 MPa):

$$mg^0 = (30 - 8.5 \times D)\sqrt{p} \qquad \text{(Eq 3)}$$

where D is grit size (mm), p is air pressure (MPa), and the factor $(30 - 8.5 \times D)$ is determined by linear regression.

The grit flow rate is lower with the STM than with the PTM (e.g., for the 1.4 mm grit, 3.2 kg/h at 0.7 MPa with the STM compared to 21 kg/h at the same pressure with the PTM). However, whatever the blasted material, within the precision of the measurements, the R_a obtained at 0.7 MPa with the STM was the same as that obtained with the PTM at 0.3 MPa. At that pressure mg^0 was only 13 kg/h with the PTM, compared to 3.2 kg/h with the STM at 0.7 MPa. The difference in mass flow rate can be explained thusly: With the STM the grit is entrained by the airflow suction, which is not very efficient, whereas with the PTM the grit is directly entrained by the air from the pressurized tank where the grit is stored. Thus, the PTM is more effective and efficient than the STM, since higher velocities are imported to the abrasive to offer a greater cutting action. Pressure-type machines are more convenient for large jobs that require high production rates or to roughen very hard surfaces because more grit can be entrained than with STMs. All the following results were obtained with the PTM (except for nozzle wear and blasting angle), since this was the more efficient machine.

3.2 *Nozzle Wear*

Nozzle wear must be checked continuously because it can be significant. It increases drastically with grit size and blasting pressure. With the STM, for example, after 50 h working time at 0.7 MPa with a 1.4 mm grit, a B_4C nozzle ID reaches 9.1 mm compared to an initial ID of 8 mm. The consequences of such wear are an almost 40% increase in the grit flow rate and a 20% decrease of the obtained R_a.

3.3 *Blasting Angle*

According to the study conducted by Wingren (Ref 7) on Inconel 718 substrates, there is a slight reduction of the grit residue and R_a when the grit blasting angle, θ, is 45° rather than 90°. Figure 6 shows the evolution of R_a versus θ with a STM at a blasting pressure of 0.8 MPa. For the three substrate materials, it can be seen that the decrease of θ below 60° results in a significant reduction of R_a for soft materials.

3.4 *Surface Hit by the Grit Particles*

Blasting time, which is an important parameter (Ref 7, 14), depends on nozzle/substrate relative velocity, internal diameter φ of the nozzle, air pressure, and diameter d_i of the surface hit by the particles, which itself is a function of the spray distance d.

The evolution of d_i with d has been measured for a blasting pressure of $p = 0.3$ MPa and three grit sizes by blasting a surface (AU4G or FT25) positioned at different distances from the fixed nozzle. The blasting time of 3 s was determined by a screen intercepting the grit flow and moved with a pneumatic jack. Figure 7 presents the results obtained with a PTM. The same curve was obtained with 0.5 MPa. It can be seen, according to the precision of the measurements (±3 mm), that d_i varies linearly with d and is almost insensitive to the grit size and the two blasting pressures.

4. Parameters That Influence R_a and R_t

4.1 *Choice of Blasting Time*

As already shown by different authors (Ref 7, 14), the influence of blasting time, t_b, is significant; below a critical value, t_{bc}, R_a varies significantly with t_b and its reproducibility is poor. For $t > t_{bc}$ the surface is overblasted. Finally, a time t_s has been chosen that, for the different tested materials, corresponds to the beginning of the plateau of the evolution of R_a with blasting time (Ref 7). It was obtained by adjusting the translation velocity to 14 mm/s ($t_s \sim 3$ s). This blasting time was almost insensitive to the studied pressures (0.2 to 0.7 MPa) and blasting distances (between 100 and 150 mm). In the following, n passes correspond to a blasting time of $3n$ s.

4.2 *Blasting Distance*

The influence of blasting distance is illustrated in Fig. 8(a), (b), and (c), respectively, for AU4G, FT25, and 100C6. These figures show that, for a given material, R_a increases with the blasting distance, d, up to 100 mm, remains almost constant up to 150 mm, and then decreases again for higher values of d. The dispersion increases slightly with d, and the plateau is slightly broader with hard materials. When d is too short, the rebounding particles reduce the number and/or the efficiency of impacting grit particles with which they collide in flight. When d is too large, the particle velocity decreases, especially for small particles that have low inertia.

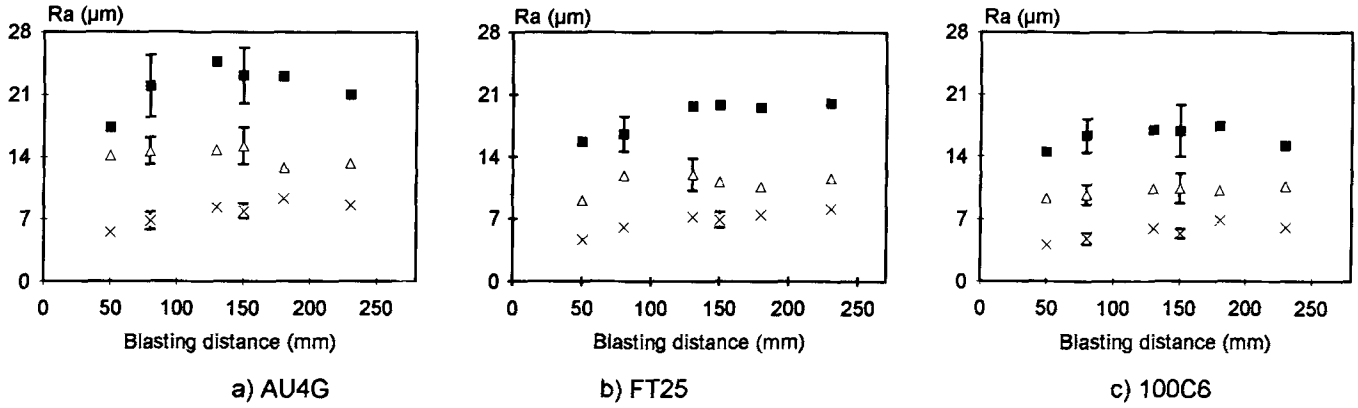

Fig. 8 Influence of blasting distance, d, on R_a for three grit sizes and three substrate materials ($p = 0.3$ MPa, one pass, PTM); ■ = 1.4 mm, Δ = 1 mm, × = 0.5 mm

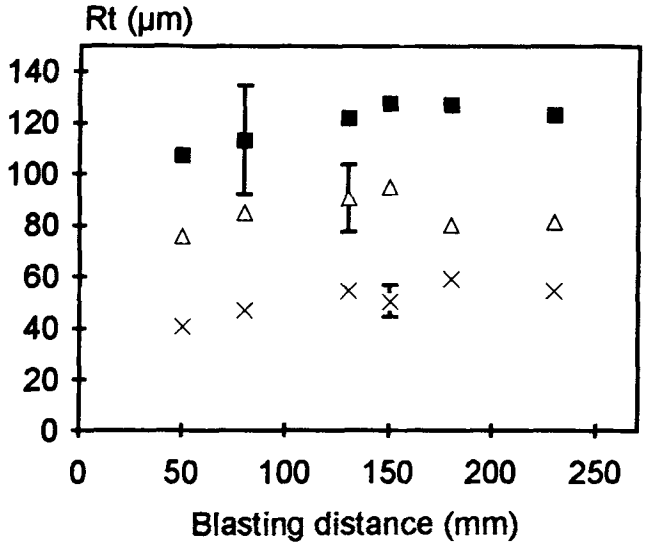

Fig. 9 Influence of blasting distance, d, on R_t for three grit sizes (p = 0.3 MPa, one pass, PTM); ■ = 1.4 mm, Δ = 1 mm, × = 0.5 mm

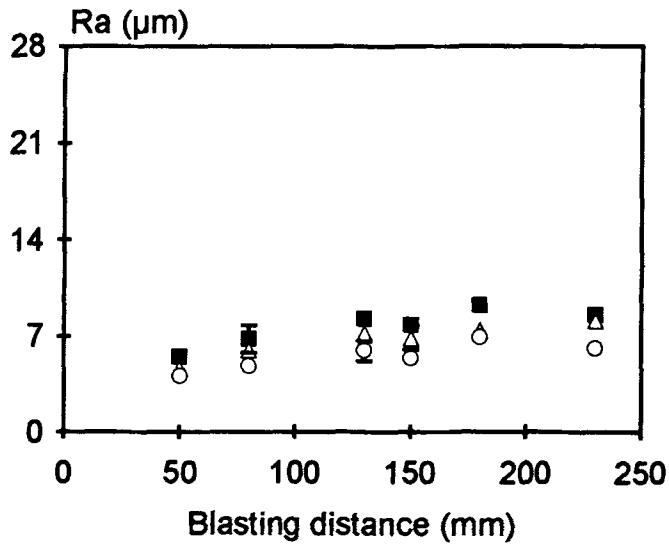

Fig. 10 For a 0.5 mm grit, evolution of R_a with d for three substrate materials ($p = 0.3$ MPa, one pass, PTM); ■ = AU4G, Δ = FT25, O = 100C6

The results are more dispersed when considering R_t, as illustrated in Fig. 9 for AU4G. The smallest grit has no significant influence on the different values of R_a obtained for the three different materials in Fig. 10.

4.3 *Blasting Pressure*

Figure 11 shows the influence of blasting pressure on R_a for two substrate materials and two grit sizes. Whatever the substrate, the influence of pressure on R_a is very low, but as will be shown later, grit wear increases drastically with p.

4.4 *Grit Size*

Grit size has the most important influence on R_a; Fig. 12 indicates a linear relationship. The value of R_a decreases slightly when the substrate Young's modulus increases. Note that when the grit size increases, the number of peaks and undercuts for a given mean length, l, decreases, and their height or depth increases. This can be seen by measuring the ratio, R, of the length l of the real surface cross section to the length l_m of the corresponding flat surface (before grit blasting). R varies between 2.4 and 2.7, this last value being obtained with the largest grit. Note that the smallest grit leads to more uniform surface asperities and low values of average dispersion of R_a and R_t.

Table 3 Deflection and curvature due to grit blasting of 34CD4 flat beams ($2 \times 20 \times 100$ mm^3)
p = 0.3 MPa, d = 130 mm, PTM, mean value of ten measurements.

Grit size, mm	Deflection, mm	Curvature, m
One pass		
0.5	0.32 ± 0.07	2.76 ± 0.52
1.0	0.66 ± 0.05	1.28 ± 0.09
1.4	1.08 ± 0.15	0.8 ± 0.11
Two passes		
0.5	...	...
1.0	0.84 ± 0.06	1.02 ± 0.08
1.4	1.12 ± 0.11	0.76 ± 0.07
Four passes		
0.5	0.37 ± 0.05	2.37 ± 0.45
1.0	1.07 ± 0.05	0.78 ± 0.04
1.4	1.56 ± 0.02	0.54 ± 0.01

4.5 *Blasting Time*

The blasting time was varied by increasing the number of passes, one pass corresponding to the time t_s defined in section 4.1. Figure 13 shows the evolution of R_a with the number of passes. With the 1.4 mm grit size on the AU4G substrate, R_a varies very little up to the sixth pass, the drop being very important at the seventh pass, which corresponds to the smoothing of the peaks due to the hardening of the material below the surface with the increase of the compressive residual stresses (see section 5). Similar behavior is observed with the FT25 substrate, but with a lesser decrease. With the hard 100C6, the same trend is observed, but only after ten passes. With the smallest grit, R_a decreases very slowly with the number of passes for the three substrate materials. The decrease of R_a is also regular with the intermediate-size grit. As will be shown in section 5, the compressive residual stresses generated below the substrate surface are less important with the 0.5 and 1 mm grit sizes than with the 1.4 mm grit.

When considering the variation of R_t for AU4G and 100C6 (Fig. 14a and b, respectively), the same behavior as for R_a is observed, but with more dispersion in the results.

5. Generation of Compressive Stresses

The measurement of residual stresses has been performed by using the incremental hole drilling method for one blasting condition of a cast iron FT25 sample (see Fig. 15). The curvature of

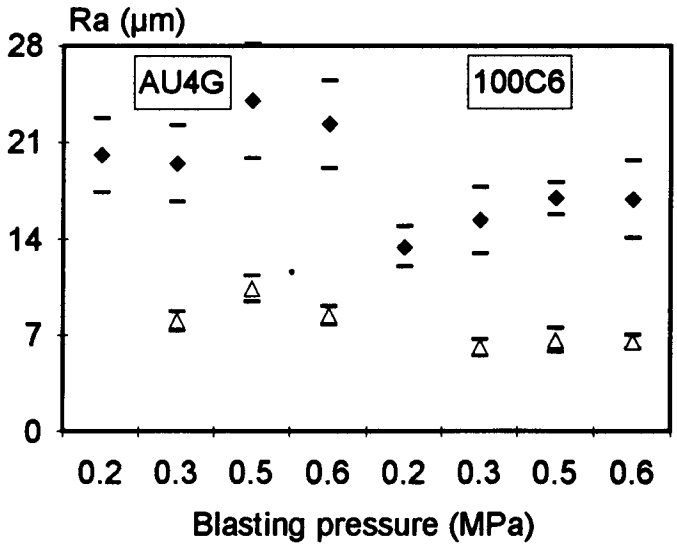

Fig. 11 Influence of blasting pressure, p, on R_a for two substrate materials (d = 130 mm, one pass, PTM); ◆ = 1.4 mm, Δ = 0.5 mm

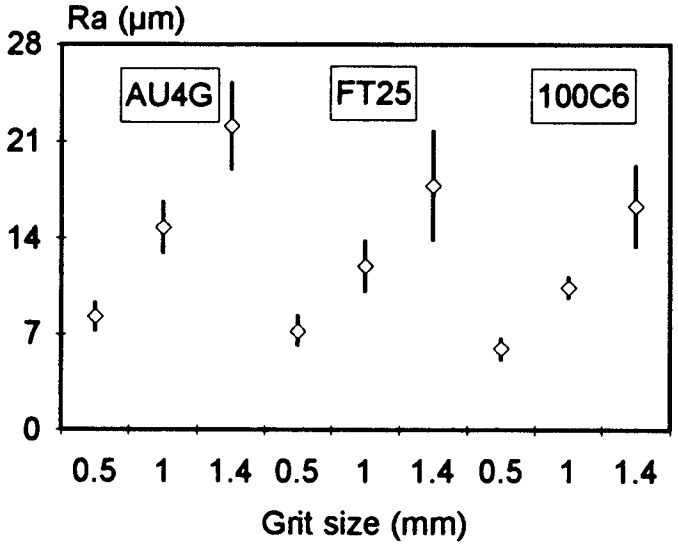

Fig. 12 Influence of grit size (0.5, 1, and 1.4 mm) on R_a for three substrate materials (p = 0.3 MPa, d = 130 mm, one pass, PTM)

flat beams was measured for 34CD4 steel alloy. The stress values obtained are only comparative (the highest deflection or the lowest curvature corresponding to the highest residual stress), since the depth of the plastically deformed zone was unknown.

Figure 15 shows the residual stress distribution within a cast iron FT25 substrate, grit blasted with 0.5 mm white alumina. Compressive residual stresses were generated and distributed within a thin layer beneath the grit-blasted substrate surface (0.4 mm in Fig. 15). The maximum stress, corresponding to the depth of the plastic zone, was reached at 0.05 mm from the substrate surface. The magnitude as well as the depth of the zone affected by the grit blasting are strongly dependent on the blasting conditions (particularly the impact pressure and the size of the particles) and on the Young's modulus of the substrate material.

The deflection and curvature of 34CD4 flat beams for different blasting times (or number of passes), three alumina grit sizes, and a grit blasting pressure of 0.3 MPa are shown in Table 3. The stresses are proportional to the induced deflection and inversely proportional to the resulting curvature of the flat beam. Each result is a mean value of ten measurements for each condition.

For comparison, assuming that the Young's modulus of 34CD4 is that of FT25, a deflection of 0.32 mm corresponds approximately to the stress distribution shown in Fig. 15. From Table 3, it is seen that the use of larger grits increases the deflection. The influence of the number of passes (n) becomes appreciable for the larger grit size. However, for $n \geq 6$ to 10 (6 for the lower Young's modulus substrate), such changes become almost negligible, in good agreement with the results shown in Fig. 13. An increase of the pressure from 0.3 to 0.5 MPa results in an increase of the compressive stresses, especially for the largest grit particles (see Table 4).

6. Grit Wear

In the preceding sections, grit blasting was always performed with a new grit, without recycling. This section examines grit

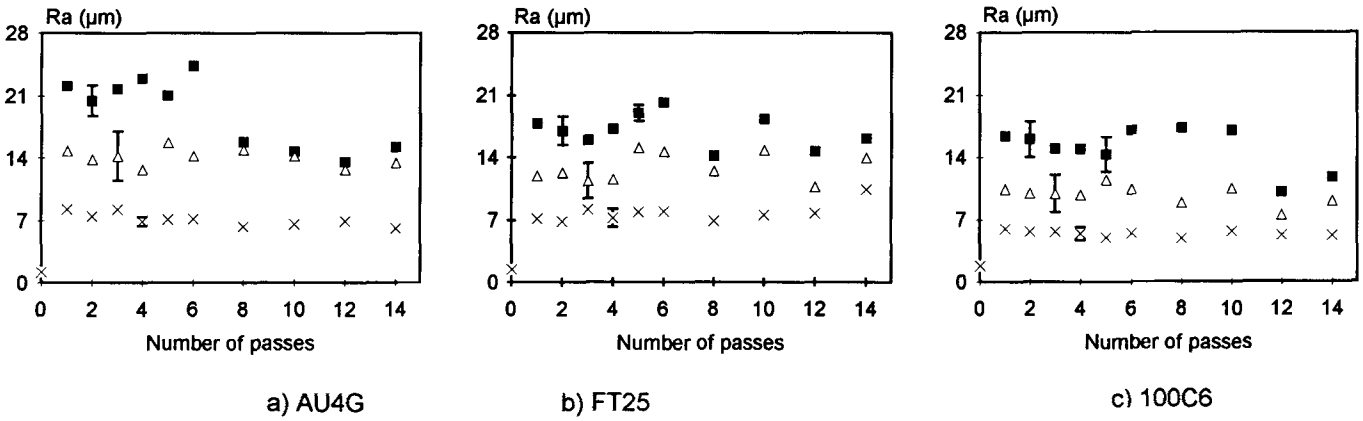

Fig. 13 Influence of number of passes on R_a for three grit sizes (p = 0.3 MPa, d = 130 mm, PTM); ■ = 1.4 mm, Δ = 1 mm, × = 0.5 mm

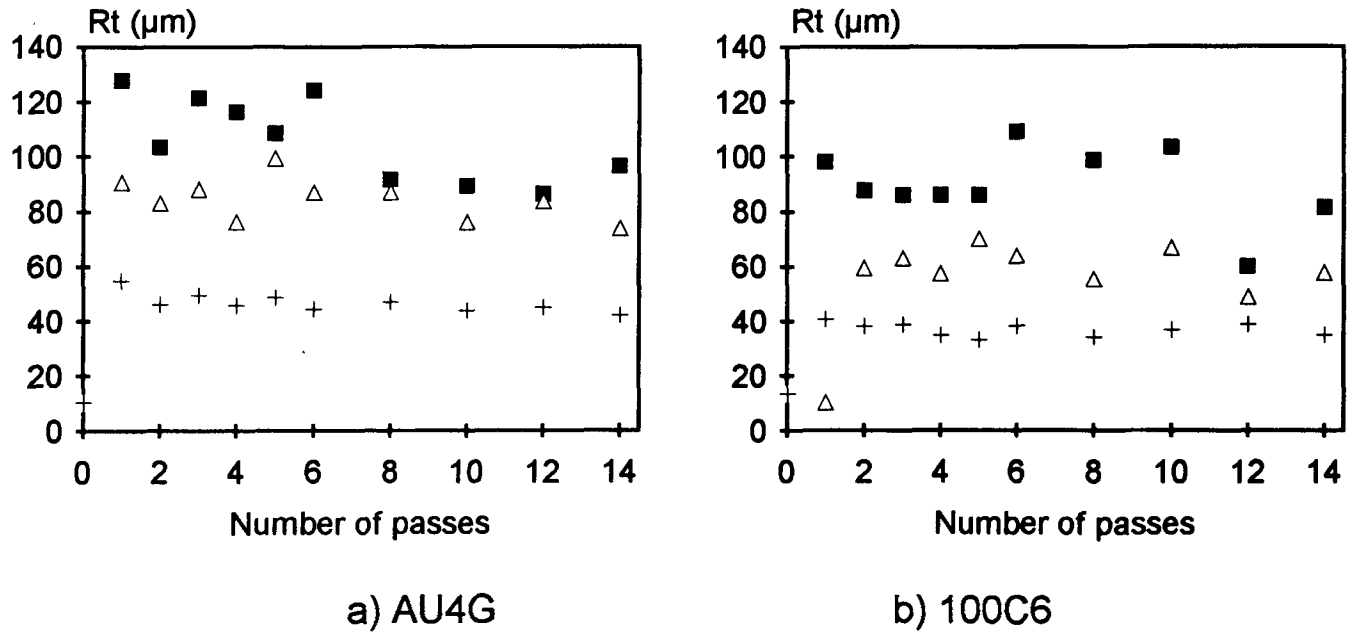

Fig. 14 Influence of number of passes on R_t for three grit sizes (p = 0.3 MPa, d = 130 mm, PTM); ■ = 1.4 mm, Δ = 1 mm, × = 0.5 mm

wear with blasting pressure and the consequences on roughness. The grit wear has been measured by a sieve analysis after each cycle. No influence of the substrate was detected on the grit wear presented in section 6.1.

6.1 *Evolution of Grit Size Distribution*

Figure 16 represents three grit distributions after one pass (one cycle) for three blasting pressures. The fragmented grit is important, especially for the largest particles, and a single pass significantly increases the quantity of small particles, particularly when blasting pressure increases. The grit fragmentation increases with the number of passes, as shown in Fig. 17.

The mean grit size decreases rapidly during the first three cycles. Table 5 summarizes the percentage of wear after one and five cycles for three pressures. Wear is greatest for the largest grit size, and it increases with blasting pressure and number of cycles.

Table 4 Deflection and curvature due to grit blasting of 34CD4 flat beams ($2 \times 10 \times 100$ mm^3)
d = 130 mm, one pass, PTM.

Grit size, mm	Deflection, mm	Curvature, m
0.3 MPa		
0.5	0.32 ± 0.07	2.76 ± 0.52
1.0	0.66 ± 0.05	1.28 ± 0.09
1.4	1.08 ± 0.15	0.8 ± 0.11
0.5 MPa		
0.5	0.43 ± 0.03	1.93 ± 0.13
1.0	0.75 ± 0.04	1.13 ± 0.06
1.4	1.89 ± 0.06	0.45 ± 0.01

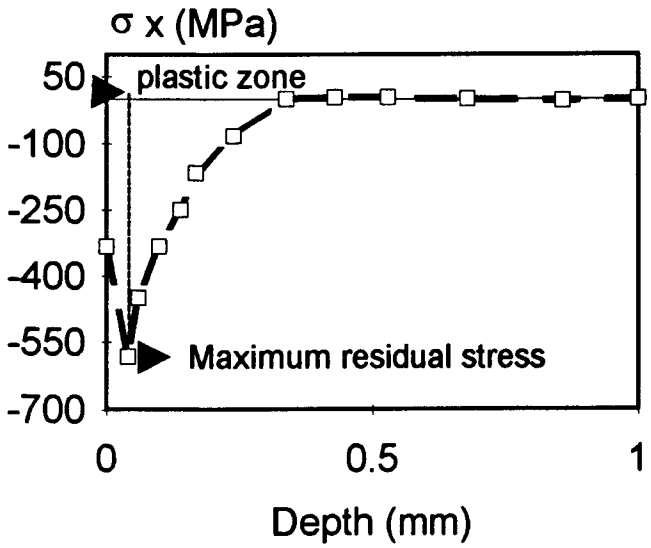

Fig. 15 Residual stress distribution within a cast iron FT25 blasted substrate (p = 0.3 MPa, d = 130 mm, t_s = 4 s, white Al_2O_3 D = 0.5

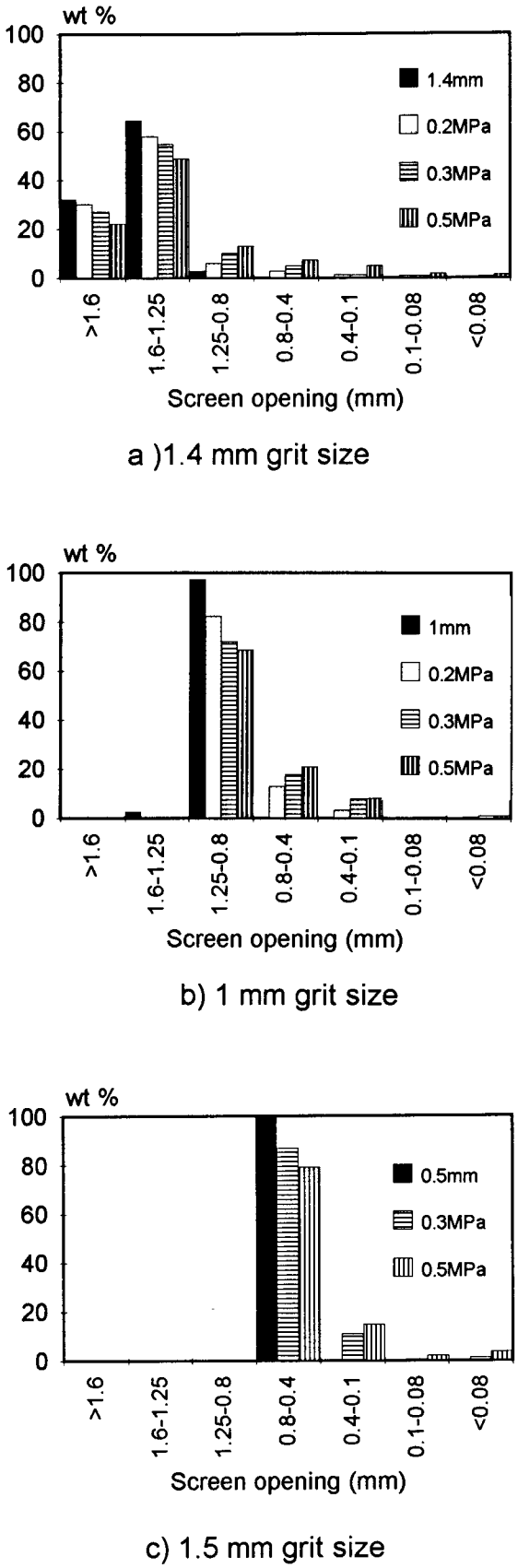

Fig. 16 Evolution of the grit size distribution after one cycle (3 s) for different blasting pressures. Black bars correspond to the initial size distribution (d = 130 mm, PTM)

6.2 *Grit Wear and Substrate Roughness*

Figure 18 shows the influence of the number of cycles on the roughness (R_a) of two substrates (AU4G and 100C6) for three pressures (note that the substrates were changed after each cycle). The results indicate that R_a diminishes with grit size due to its wear. This influence is more significant for the softest material and less sensitive for the smallest grit.

7. Grit Residue

The sample surfaces were grit blasted with the three white alumina grit sizes for the same blasting time (four passes), distance (130 mm), and pressure (0.3 MPa) and were then cleaned prior to analysis. The cleaning procedure was the same as that described in section 2.6. Without cleaning, the grit residue was more than twice that measured after cleaning.

The residue measurements indicated that the difference between $\theta = 60°$ and $\theta = 90°$ is not critical (on the order of 5%). In the following, all measurements presented were performed with $\theta = 90°$.

Figure 19 shows the evolution of grit residue with respect to the grit size of alumina on the blasted surface of XC38 steel substrates. It can be seen that the grit residue increases with the grit size (1% for a 0.5 mm grit size compared to 7% for a 1.4 mm grit).

The grit residue increases with blasting pressure and time (Ref 7, 14) due to the higher energy and flow of the grit blasting particles. Note that compared to the initial grit sizes, the grit residues are mostly fragmented particles with a mean size less than a few tenths of the initial size. The increase of the grit residue with grit size is due to an increase in grit fragmentation with respect to grit size, and the small particles (a few tenths of the initial size) resulting from the fragmentation are embedded within the undercuts by the impact of the large grit particles. According to the results of Yankee et al. (Ref 14), who studied the influence of the cleaning procedure (ultrasonic method or air blasting) on the grit residue, the ultrasonic method seems to be the better. Nevertheless, the results obtained with a combination of these two methods indicate that the grit residue cannot be completely eliminated and that new techniques should be developed.

Table 5 Percentage of grit wear after one and five cycles

Grit size, mm	Grit wear, %	
	1 cycle	5 cycles
0.2 MPa		
0.5	...	...
1.0	9	27
1.4	17	39
0.3 MPa		
0.5	13	31
1.0	15	40
1.4	28	66
0.5 MPa		
0.5	20	44
1.0	26	60
1.4	31	77

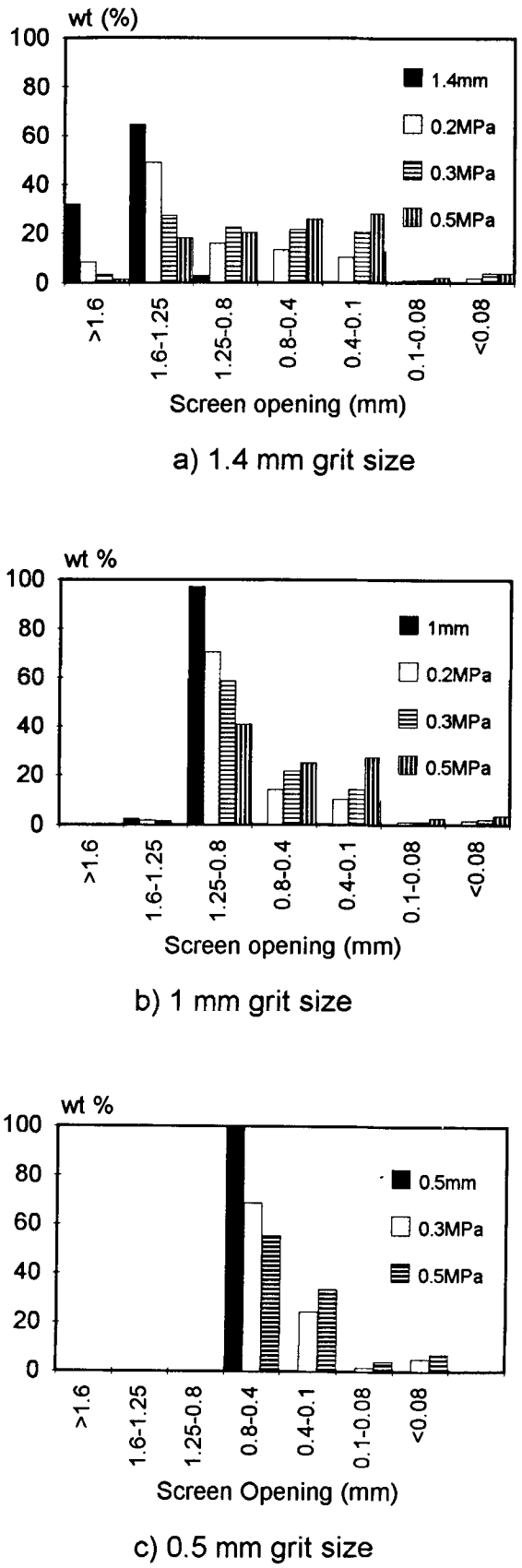

Fig. 17 Evolution of the grit size distribution after five cycles for different blasting pressures. Black bars correspond to the initial size distribution (d = 130 mm, PTM)

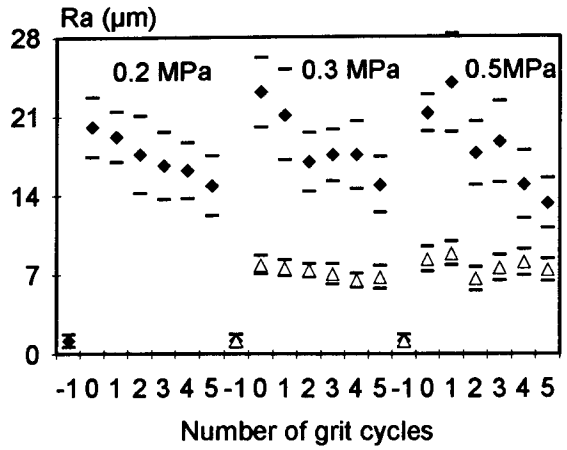

a) AU4G substrate

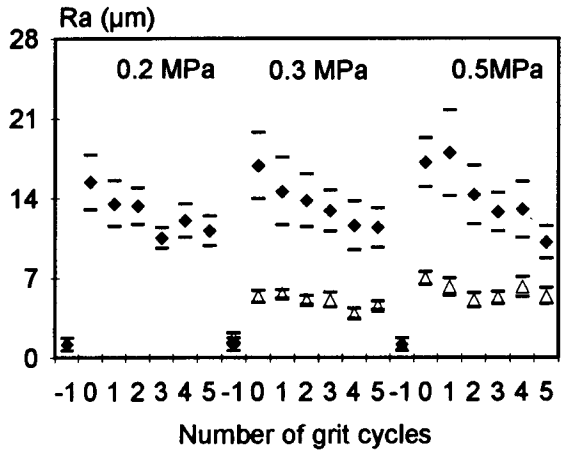

b) 100C6 substrate

Fig. 18 Influence of the number of grit cycles on R_a for two grit sizes (◆ = 1.4 mm and Δ = 0.5 mm) and three pressures. Cycle −1 = initial roughness of the substrates; cycle 0 = first pass. (d = 130 mm, PTM)

In good conjunction with the results presented in section 6, the grit residue increased with:

- *Blasting pressure:* for example, by 10% with 0.5 MPa compared to 7% with 0.3 MPa (1.4 mm grit)
- *Number of grit cycles:* by about 60% for five cycles compared to one cycle
- *Number of passes* (with a new grit at each pass): from 7% with four passes to 9% with 18 passes (1.4 mm grit)

8. Conclusions

A systematic study of grit blasting parameters was made for three different substrate materials: aluminum alloy AU4G, cast iron FT25, and hard steel 100C6. The study focused on a PTM using a boron carbide nozzle of 8 mm ID. White alumina grit of three sizes (0.5, 1, and 1.4 mm in mean diameter) was used. The

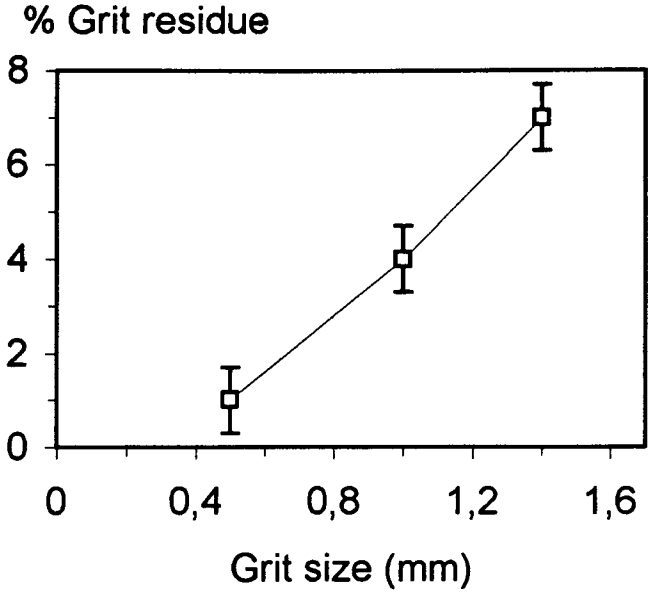

Fig. 19 Evolution of grit residue (% area surface) with grit size (p = 0.3 MPa, d = 120 mm, four passes, PTM)

influence of the different blasting parameters on the resulting roughnesses (R_a and R_t), grit residues, and induced residual stresses was studied.

The PTM was by far the most efficient, similar results being obtained with pressures 2.5 times lower than with the STM, all other blasting parameters being constant. However, the grit flow rate was three to four times higher with this machine for the same nozzle internal diameter.

The results for the different blasting parameters are:

- *Blasting time,* t_b: Below a critical value, t_{bc} (in our experiments, close to 3 s), R_a varied drastically with t_b; above t_{bc}, R_a, and R_t reached a plateau.
- *Grit size, D*: R_a and R_t increased almost linearly with D, the highest slopes being obtained with the materials having the lowest Young's modulus.
- *Blasting distance*: Almost no influence between 80 and 150 mm
- *Blasting angle*: Little significance, provided it was between 60° and 90°
- *Blasting pressure*: Roughness did not increase much with pressure, while the grit flow rate increased with the square root.

Grit blasting induced very high compressive stresses below the blasted surface due to plastic deformation of the material. The affected zone and the value of the compressive peak increase strongly with grit size, blasting pressure, and blasting time. Therefore, depending on the Young's modulus of the material, after a given number of passes the roughness decreased, the peak being smoothed due to material hardening below the blasted surface.

The grit residue depended on the grit fragmentation and was enhanced by increasing grit size and blasting pressure. Residue increased from 1% with a 0.5 mm grit to 7% with a 1.4 mm grit.

When the quantity of fragmented particles increased (i.e., when the grit was recycled without sieving), the grit residue increased from 7% with one cycle to 11% with five cycles for the 1.4 mm grit.

This grit residue can negatively affect coating adhesion. For example, when alumina and zirconia were sprayed on cold substrates (Ref 6), the adhesion increased almost linearly with R_a, but its maximum value was below 20 MPa. However, when sprayed on substrates preheated at 300 °C without oxidation, the adhesion was highest (~60 MPa) on surfaces of R_a between 3 to 5 μm (i.e., as obtained with 0.5 mm white alumina grit) (Ref 6). The adhesion decreased when the R_a increased. This occurred in conjunction with an increase of grit residue and residual stresses.

In conclusion, the best way to improve ceramic coating adhesion is a substrate roughness below 5 μm R_a obtained with a small alumina grit size and a low blasting pressure.

References

1. *Thermal Spraying,* American Welding Society, 1985
2. J.M. Zaat, Thermal Spraying, *Ann. Rev. Mater. Sci.,* Vol 13, 1983, p 9-42
3. S. Kitahara and A. Hasui, A Study of the Bonding Mechanism of Sprayed Coatings, *J. Vac. Sci. Technol.,* Vol 11 (No. 4), 1974, p 747-753
4. C.P. Bergmann, Preheating of Substrate as Adherence Agent of Plasma Sprayed Coatings, *Thermal Spraying '93,* D. Von Hofe and E. Lugsheider, Ed., DVS, Düsseldorf, 1993, p 114-118
5. W. Funk, F. Coebe, and M. Manz, The Influence of Substrate Temperature on the Bond Strength of Plasma Sprayed Oxide Ceramics, *1st Plasma-Technik Symp.,* Vol 1, H. Eschnauer, P. Huber, A.R. Nicoll, and S. Sandmeier, Ed., P.T. Wohlen, 1988, p 59-66
6. M. Mellali, P. Fauchais, and A. Grimaud, Influence of Substrate Roughness and Temperature on Alumina Coatings Adhesion-Cohesion, *Surf. Coat. Technol.,* Vol 81 (No. 2-3), 1996, p 275-286
7. J. Wiggren, Grit Blasting as Surface Preparation before Plasma Spraying, *Thermal Spray: Advances in Coating Technology,* D. Houck, Ed., ASM International, 1988, p 99
8. C. Beauvais, Surface Preparation, Introduction, Surface Treatment, *J. Techniques de l'Ingénieur,* Metallurgie-M5, 1982, p 1435
9. J.J. Dupras and G. Garnier, Chemical Decreasing, Surface Treatment, *J. Techniques de l'Ingénieur,* Metallurgie-M5, 1982, p 1450
10. R.L. Apps, The Significance of Surface Preparation and Flame Spraying of Metals, *Chem. Eng.,* Vol 292, 1974, p 769-773
11. D.M. Karpinos, V.G. Zil'Bergerg, A.M. Vyal'Tsev, and V.S. Kud, Shot Blasting as Means of Preparing Surfaces for Plasma Deposition, *Powder Metall. Mater. Parts Coat.,* 1979, p 675-678
12. S. Amada, H. Yamada, S. Yematsu, and Y. Saotome, Modelling and Measurements of Adhesive Strength of Thermal Spray Coatings, *Thermal Spray: International Advances in Coatings Technology,* C.C. Berndt, Ed., ASM International, 1992, p 915-920
13. S. Amada and Y. Yamada, Introduction of Fractal Dimension to Adhesive Strength of Plasma Sprayed Coatings, *11th Int. Symp. Plasma Chemistry,* Vol 1, J. Harry, Ed., Loughborough, U.K., 1993, p 150-155
14. D.H. James, A Review of Experimental Findings in Surface Preparation for Thermal Spraying, *J. Mech. Work. Technol.,* Vol 10, 1984, p 221-232
15. S.J. Yankee, R.L. Salsbury, and B.J. Pletka, Quality Control of Hydroxylapatite Coatings: The Surface Preparation Stage, *Thermal Spray Coatings: Properties, Processes and Applications,* T.T. Bernecki, Ed., ASM International, 1991, p 475-481
16. M. Mellali, "Influence of Roughness and Temperature of Substrates on Adhesion/Cohesion and Residual Stresses of Plasma Sprayed Alumina Coatings," Ph.D. thesis, University of Limoges, France, 18 July 1994
17. C. Richard, "Study of Mechanical Characteristics of Thermal Spray Coatings," Ph.D. thesis, University of Technology of Compiègne, France, 18 Dec 1992
18. J. Lu, A. Niku-Lari, and J.F. Flavenot, Measurement of the Through Thickness Stress Distribution by the Incremental Hole Drilling Method, *Mèm. Etud. Sci. Rev. Mètall.,* 1985, p 69-81
19. D.J. Greving, V.R. Shadleg, and E.F. Rybicki, Effects of Coatings Thickness and Residual Stresses on Bond Strength of C633-79 Thermal Spray Coating Test Specimens, *Thermal Spray Industrial Applications,* C.C. Berndt and S. Sampath, Ed., ASM International, 1994, p 639-645